

# Hydrogenation of CO<sub>2</sub> over Co supported on carbon nanotube, carbon nanotube-Nb<sub>2</sub>O<sub>5</sub>, carbon nanofiber, low-layered graphite fragments and Nb<sub>2</sub>O<sub>5</sub>



Obid Tursunov <sup>a,\*</sup>, Zaid Tilyabaev <sup>b</sup>

<sup>a</sup> The Laboratory of Nanochemistry and Ecology, National University of Science and Technology MISiS, Moscow, Russian Federation

<sup>b</sup> The Laboratory of Fine Organic Synthesis, Sadykov Institute of Bioorganic Chemistry, Tashkent, Uzbekistan

## ARTICLE INFO

### Article history:

Received 10 November 2017

Received in revised form

17 December 2017

Accepted 18 December 2017

Available online 26 December 2017

### Keywords:

CO<sub>2</sub> hydrogenation

Catalyst

Support

Carbon nanotubes

## ABSTRACT

CO<sub>2</sub> hydrogenation was studied with catalysts containing 1.5–35 wt% Co supported on carbon nanotubes, nanofibers, low-layered graphite fragments and composites of carbon nanotube-Nb<sub>2</sub>O<sub>5</sub>. All catalytic processes with Co/supported catalysts were investigated using XRF, DSC, TGA, H<sub>2</sub>-TPR, TEM, SEM and XPS. Based on obtained results, it is indicated that the products from CO<sub>2</sub> hydrogenation were CH<sub>4</sub> and/or CO under reaction conditions pressure of 1.5 MPa and temperature of 200–500 °C, as well as the size of the particles of Co and their phase state directly affected on the catalysts activity. 3 wt% Co catalyst supported on carbon nanotubes has shown catalytic inactivity due to amorphous state of metal. It is possible to activate them during Co crystallization after thermal treatment. It is shown, that the size of Co particles supported on carbon nanotubes is 4–6 nm. The methods of fictionalization of the surface of carbon nanomaterials ensuring an additional stability of metal nanoparticles is recommended.

© 2017 Energy Institute. Published by Elsevier Ltd. All rights reserved.

## 1. Introduction

Since few years, rapid climate change and global warming have attracted an essential attention of scientists and the leaders of not only developed but also developing countries, and this statement can be assured by recent two world summit on climate change (Warsaw 2013 and Paris 2015) which involved the leaders from more than 50 countries. Carbon dioxide (CO<sub>2</sub>) emission is one of the prominent reasons for the above mentioned global issues due to its constant expansion in the atmosphere in the result of quicken growth in wide-scale consumption of carbon-based energy globally. Consequently, the pursue for cleaner and renewable energy sources to fulfill the quick economic and population growth has become more challenging since a few decades. According to American Chemical Society (ACS), the global CO<sub>2</sub> emission from the use of large scale industrial applications and fossil fuels has reached to about 36 billion tones in 2013. Le Quere et al. (2016) also stated that averaged over the last decade, CO<sub>2</sub> emissions from various types of fossil fuels and industry account for approximately 91% of man-caused emissions of CO<sub>2</sub>. Consequently, 9.9bn tones of carbon in the form of CO<sub>2</sub> emitted from fossil fuels in 2015, 41% came from coal, from oil 34%, from gas 19% and from cement production 5.6% [1](see Fig. 1).

Hue et al. (2013) [2] reported that fossil fuel consumption has caused atmospheric concentration of CO<sub>2</sub> increases from 280 parts per million (ppm) in pre-industrial times to 382 ppm in 2006 and the atmospheric concentration of CO<sub>2</sub> is still steadily amplifying at a rate of about 1.9 ppm/year.

However, as long as we're emitting CO<sub>2</sub>, it continues to accumulate in the atmosphere and it is doing so at record levels. Hence, the robust technologies such as carbon capture and storage (CCS), and carbon capture and utilization (CCU) for CO<sub>2</sub> are required in a wide-scale [2]. However, CO<sub>2</sub> is considered the most abundant carbon source in the atmosphere; it can be applied as a nonpoisonous and an inexpensive C1 building block in chemical reactions and processes [3,4]. Additionally, significant efforts have been made to prevent the critical accumulation of CO<sub>2</sub> in the atmosphere by the reduction of carbon dioxide into different useful chemical liquid products in the recent years. The CO<sub>2</sub> conversion to value-added fuels using non-carbon based energy sources (e.g. wind, solar, geothermal, or nuclear) is considered as greatly

\* Corresponding author.

E-mail address: [obidtursunov@gmail.com](mailto:obidtursunov@gmail.com) (O. Tursunov).

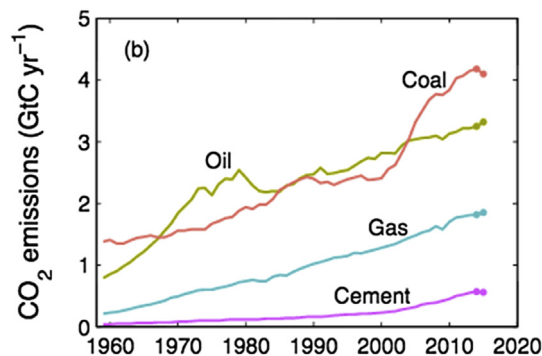


Fig. 1. Global CO<sub>2</sub> emissions by fuel type [1].

challenging, but is expected to be a verily alternative in order to reduce carbon dioxide emission [5]. There are several mechanisms for CO<sub>2</sub> conversion into liquid chemicals/fuels such as biological fixation, solar driven photochemical reduction, electrochemical conversion and thermo-chemical catalytic conversion or hydrogenation [6,7].

Hydrogen is a high energy material and it can be directly applied as the reagent for transformation of CO<sub>2</sub>. The basic products from hydrogenation of CO<sub>2</sub> can be categorized into two groups: chemicals and fuels. CO<sub>2</sub> hydrogenation products like methanol, dimethyl ether, hydrocarbons, methane etc. are classy and profitable fuels [8,9] in application for various internal combustion engines, as well as there are simple for transportation and storage. In recent years, CO<sub>2</sub> Hydrogenation process has been thoroughly researched because of practical and fundamental importance in the field of catalysis, biology, nanotechnology, nano-science, surface science and undoubtedly environmental science. However, there are several critical issues connected with utilization of CO<sub>2</sub> due to its high thermodynamic and kinetic stability with high oxidation state of carbon. The most efficient way to surmount such complications could be catalytic applications for CO<sub>2</sub> hydrogenation process.

Reductive conversion of CO<sub>2</sub> (Fischer-Tropsch synthesis) is considered as one of the effective methods to obtain liquid hydrocarbons or fuels. The Fischer–Tropsch (FT) process is a collection of chemical reactions that converts a mixture of carbon monoxide and hydrogen into liquid hydrocarbons. Consequently, the cost of the FT process depends on the cost of chemical used during the reaction process. These reactions occur in the presence of certain metal catalysts, basically at temperatures of 150–500 °C and pressures of one to several tens of atmospheres. Hence, using a multifunctional catalyst has the potential to reduce costs of the FT process. As well as, the synergistic integration of intensified unit operations with chemical reaction leads to enhanced catalyst performance and significant economic advantages of the FT process [10–12].

A few group VIII metals such as cobalt, iron, ruthenium and nickel are known to be active components of the Fischer-Tropsch Synthesis (FTPS) catalysts. Recently, massive research investigations have been constantly conducted to develop novel catalytic and technological solutions for the optimization of this process [10–16]. Currently, CO<sub>2</sub> is used only for large-scale production of soda, urea and salicylic acid, as well as methanol [17]. Additionally, catalytic hydrogenation of CO<sub>2</sub> could open vast technical opportunities and become perspective for production of liquid hydrocarbons – artificial fuels [17,18]. Moreover, it is well-known that CO<sub>2</sub> is converted to methane in order to eliminate CO<sub>2</sub> from technological gases in the industry [19]. Cobalt and iron based catalysts are considered as more perspective catalysts for production of hydrocarbons from CO<sub>2</sub> hydrogenation [20]. Particularly, supported Co catalysts have considerable merits and are known for their selectivity and activity towards Fischer-Tropsch synthesis process and low cost, thereby making FT process more cost-effective [21,22]. Lower deactivation rate, lower water-gas shift activity, high chain growth probability and inexpensive costs turn cobalt catalysts the prominent candidates for transferring synthesis gas into value-added clean liquid fuels [23,24].

This work is devoted to study of cobalt-containing catalysts for CO<sub>2</sub> hydrogenation and possibilities of interaction of the active phase with support and the selection of an optimal size of metallic particles.

## 2. Experimental

### 2.1. Synthesis of catalyst supports

The chemical substances used in this study were obtained from the fine chemical manufacturing company - Spectrum Chemical Mfg. Corp. and from the UK Scientific Laboratory Supplies (SLS).

Carbon nanotubes (further designated as CNT) was received using the pyrolytic decomposition of hexane at the temperature of 750 °C during 6 h in the presence of MgO with specific surface area (SSA) – 55 m<sup>2</sup>/g, impregnated by an aqueous solution of cobalt nitrate (0.1 mol %) and ammonium molybdate (0.05 mol%) in a tubular reactor (i.d., 50 mm, volumetric flow rate of carrier gas N<sub>2</sub> – 600 ml/min). Carbon nanofibers (further designated as CNF) were synthesized by pyrolytic decomposition of benzene, containing 30 wt% Fe(C<sub>5</sub>H<sub>7</sub>O<sub>2</sub>)<sub>3</sub> [25–27]. The low-layered graphite fragments (further designated as LGF) were obtained by pyrolytic decomposition of butylamine at the temperature of 800 °C for 25 min in the presence of MgO (specific surface area – 150 m<sup>2</sup>/g) [28]. Further CNT, CNF and LGF were purified from the impurities of MgO and Co or Fe by the treatment with concentrated hydrochloric acid and washed on the Buchner funnel with distilled water to a neutral value of pH and dried at 140 °C for 10 h. For the functional group modification, the surface of CNT was treated with a solution of concentrated nitric acid for 7 h then washed with distilled water to a neutral value of pH.

CNT-Nb<sub>2</sub>O<sub>5</sub> composites were obtained by pyrolytic decomposition of methane at the temperature of 650 °C for 5 h in the presence of Nb<sub>2</sub>O<sub>5</sub> preliminarily impregnated with an alcohol solution of cobalt nitrate (0.1 mol%) [29] (carbon phase content ~ 13 wt%).

**Table 1**  
Co content in prepared catalysts.

Catalyst	Support	Content of Co, wt%
3Co/CNT	CNT	3
35Co/CNT	CNT	35
3Co/CNF	CNF	3
1.5Co/LGF	LGF	1.5
3Co/LGF	LGF	3
10Co/LGF	LGF	10
10Co/CNT–Nb <sub>2</sub> O <sub>5</sub>	CNT–Nb <sub>2</sub> O <sub>5</sub>	10
20Co/CNT–Nb <sub>2</sub> O <sub>5</sub>	CNT–Nb <sub>2</sub> O <sub>5</sub>	20
35Co/CNT–Nb <sub>2</sub> O <sub>5</sub>	CNT–Nb <sub>2</sub> O <sub>5</sub>	35
10Co/Nb <sub>2</sub> O <sub>5</sub>	Nb <sub>2</sub> O <sub>5</sub>	10
20Co/Nb <sub>2</sub> O <sub>5</sub>	Nb <sub>2</sub> O <sub>5</sub>	20
35Co/Nb <sub>2</sub> O <sub>5</sub>	Nb <sub>2</sub> O <sub>5</sub>	35

## 2.2. Catalyst preparation

The catalysts were prepared by the impregnation method of the supports with a solution of cobalt nitrate. An alcoholic solution of  $\text{Co}(\text{NO}_3)_2 \cdot 6\text{H}_2\text{O}$  was poured into the sample of carbon nanomaterial CNT–Nb<sub>2</sub>O<sub>5</sub> or Nb<sub>2</sub>O<sub>5</sub> composite under vigorous stirring and processed in ultrasound bath. Afterward, the obtained sample was placed into the heated oven up to 140 °C and maintained for 10 h. The catalyst containing 1.5 wt% of Co was obtained by the method of unforced adsorption of cobalt nitrate on low-layered graphite fragments (LGF). After the sample of LGF was placed in 0.0854 g/mol solution of  $\text{Co}(\text{NO}_3)_2 \cdot 6\text{H}_2\text{O}$  under vigorous stirring for 24 h. The mother liquor was filtered off on the Buchner funnel and the cobalt content was determined from the difference in the concentrations in the initial solution and the filtrate spectrophotometrically on the JENWAY 6715UV/Vis instrument. Table 1 highlights the content of Co in the catalysts and their designation.

## 2.3. Catalyst characterization

The characterization of catalysts were determined using various testing methods, such as surface analysis, thermal analysis (TA), differential scanning calorimetry (DSC), thermogravimetric analysis (TGA), N<sub>2</sub>-physisorption, surface-sensitive X-ray photoelectron spectroscopy (XPS) and H<sub>2</sub>-temperature-programmed reduction (H<sub>2</sub>-TPR).

Surface photomicrographs of the catalysts were obtained using JEOL JSM-7610 Scanning Electron Microscope with high probe current up to 200 nA (at 15 kV) and built-in r-filter enabling user selectable mixture of secondary electron and backscattered electron images, as well as with large specimen chamber (200 mm diameter sample).

Results from the thermal analysis (TA) and differential scanning calorimetry (DSC) as well as thermogravimetric (TG) analysis were obtained using Netzsch STA 409 CD-QMS 403/5 SKIMMER, with heating rate of 5 °C.

N<sub>2</sub>-physisorption isotherms were measured at –197 °C using an accelerated surface and porosimetry system - Micrometrics ASAP 2010 BET/Porosimeter. Prior to the experimental processes, the samples were dehydrated at 100 °C until the vacuum pressure was lower than 5 μm Hg. The measurement of surface area of the prepared samples was performed using well-known Brunauer-Emmett-Teller (BET) technique for the relative pressures within the range of  $P/P_0 = 0.05–0.2$ .

Surface-sensitive X-ray photoelectron spectroscopic (XPS) test was executed using high resolution multi-technique AXIS ULTRA DLD spectrometer equipped with Al K $\alpha$  radiation (150 w, 4 mA,  $h\nu = 1486.6$  eV) under ultrahigh vacuum  $10^{-7}$  Pa. In addition, the binding energies were calibrated inwardly via adventitious carbon deposit C (1s) with  $E_b = 284.8$  eV.

H<sub>2</sub>-temperature-programmed reduction (H<sub>2</sub>-TPR) measurements were profoundly performed by using chemisorption analyzer (FINE-SORB-3010A) within the range of 50–900 °C at the 15 °C/min of heating rate under 10% H<sub>2</sub>/Ar as well as carrier gas argon, with 10 ml/min flow rate. The H<sub>2</sub> consumption was controlled using thermal conductivity detector (TCD).

## 2.4. Catalytic test

Catalytic tests were carried out using a vertical flow quartz reactor with the diameter of 18 mm, placed in a tubular furnace with the K-type thermocouple. Prior to the catalytic tests, the catalysts were pre-reduced with hydrogen (flow rate 15 ml/min) at the temperature of 400 °C for 4 h. In a number of cases, after treatment with reagent gases, the catalysts were passivated with a mixture of 2–3 vol% of O<sub>2</sub> and 96–98 vol% of Ar at normal room temperature [30–32]. CO<sub>2</sub> hydrogenation was conducted at 200–500 °C and the reactant gas flow (H<sub>2</sub>: CO<sub>2</sub>: He = 5:2:1, molar) and the total flow rate was 2.5 l/g<sub>cat</sub>h. The excurrent products (hydrocarbons) were analyzed using an online system connected with Agilent 6820 gas chromatography equipped with a two-column analytical system, the Porapak Q and molecular sieve columns, which are connected to two detectors: 1) the thermal conductivity detector (TCD) and 2) the flame ionization detector (FID), respectively. Separation and analysis of the content of CO<sub>2</sub>, CO and CH<sub>4</sub> in products was carried out using the same Agilent 6820 gas chromatograph.

## 3. Results and discussions

Fig. 2 highlights the micrographs obtained using scanning electron microscopy (SEM) and transmission electron microscopy (TEM) of all carbon-containing supports of the catalyst. According to the microscopy, CNT and the CNT–Nb<sub>2</sub>O<sub>5</sub> composite were thin tubes with an external diameter of not more than 25 nm. The carbon fibers were formed with a diameter of up to 140 nm during the synthesis without the template in the presence of iron catalyst. The carbon layers were not structured in them and contained massive edge carbon atoms [26,27].

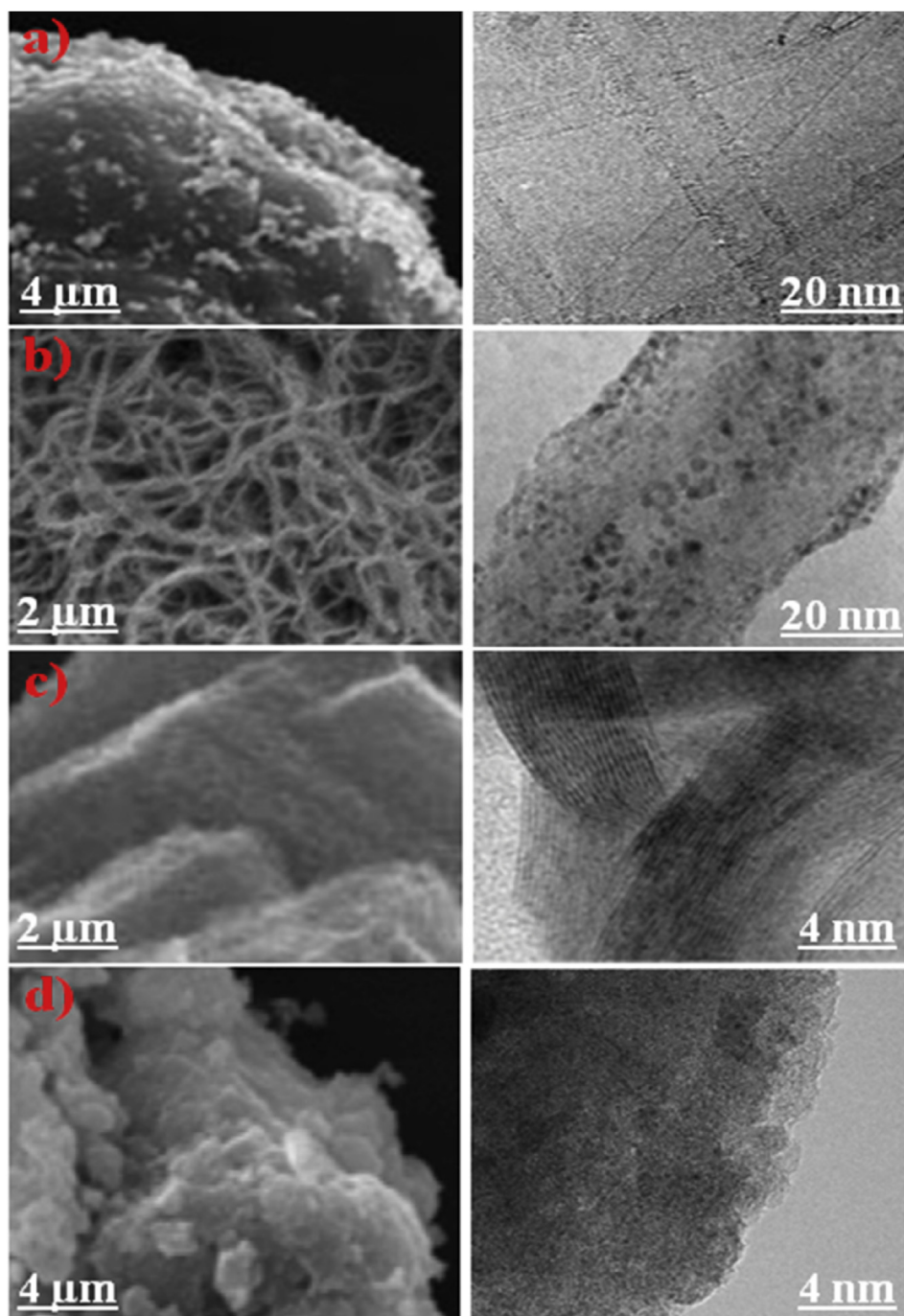


Fig. 2. SEM and TEM images of the catalysts: CNT (a), CNF (b), LGF (c) and CNT-Nb<sub>2</sub>O<sub>5</sub> (d).

LGF were characterized by a layered structure, which can be represented in the form of several (usually 6–10) piled graphene sheets and repeating the shape and the size of the template [33–35].

According to TG and DSC analysis, CNT and LGF were thermally stable up to 560–640 °C, composite of CNT-Nb<sub>2</sub>O<sub>5</sub> up to 410 °C and CNF were destroyed above 310 °C, which imposed limitations on the choice of temperature conditions during the catalytic experiments. All materials had a highly developed surface: the largest value of specific surface area (SSA) – 896 m<sup>2</sup>/g was observed in LGF. Table 2 displays the thermal properties of the supports and the data of the low-temperature nitrogen porosimetry.

To stabilize the metals on the surface of carbon materials, various approaches are frequently used (for instance, surface functionalization, introduction of heteroatoms into the carbon structure), aimed at creating centers of localization of catalytically active particles. Carbon nanotube's treatment with nitric acid [36] or hydrogen peroxide [24,37] leads to the formation of carboxyl groups on their surface, whilst the degree of functionalization depends on the time of oxidative treatment and does not exceed 12.8 at% [36]. The total oxygen content and its chemical state in the support of CNTs were determined by the XPS method (Fig. 3b) and it was 9.1 at%, and oxygen formed chemical bonds with carbon C–O (3.5 at%), C=O (3.9 at%) and COOR (0.7 at%). To form the centers of stabilization of the metal catalyst on the LGF's surface, a partial substitution of carbon atoms with nitrogen was applied in the graphene sheet structure during the synthesis. Such approach previously

**Table 2**  
Thermal and physicochemical properties of the catalyst supports.

Cat. Support	TG and DSC analysis			SSA, m <sup>2</sup> /g	Por. average radius, Å	Por. total vol., cm <sup>3</sup> /g
	endothermic/exothermic	$\Delta m$ , %	DSC effect, °C			
CNT	Endo-water loss	3.6	125	213	20	0.84
	Exo-CNT burning	91.7	560–870			
CNT-Nb <sub>2</sub> O <sub>5</sub>	Endo-water loss	1.8	103	78	23	0.24
	Exo-removal of organic fragments	0.5	125–325			
	Exo- amorphous carbon burning	2.3	360			
	Exo-CNT burning	31.2	468			
	Exo- graphite shells burning	7.0	585			
CNF	Endo-water loss	6.4	100	235	20	0.37
	Exo-CNF burning	86.9	310–630			
LGF	Endo-water loss	1.7	100	896	24	3.04
	Exo-LGF burning	97.1	640			
Nb <sub>2</sub> O <sub>5</sub>	Endo-absorbed water loss	0.3	103	191	57	0.55
	Endo-water loss	8.8	760			

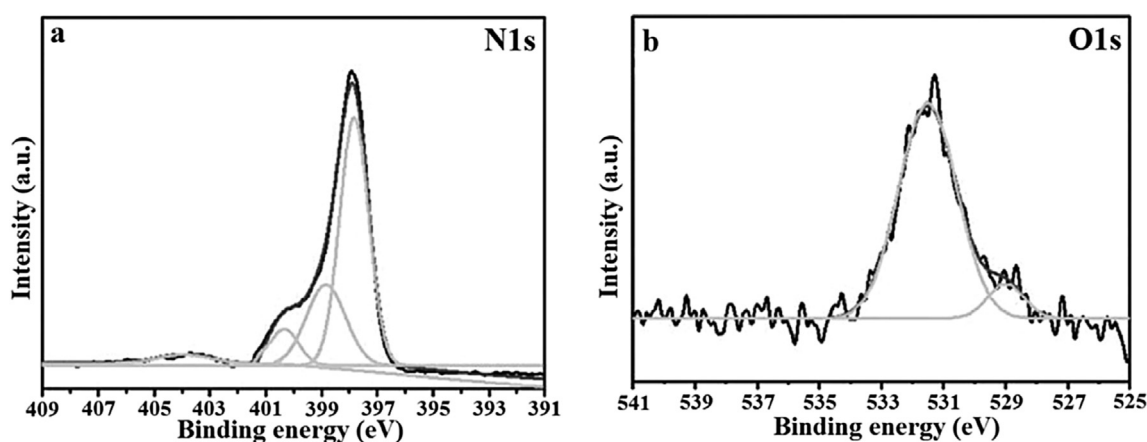


Fig. 3. XPS spectra N1s for the LGF (a) and O1s for the CNT (b).

has been used by Refs. [38,39] to obtain cobalt catalysts supported on hetero-substituted by nitrogen atoms or phosphorus of CNT for the Fischer-Tropsch process. According to the XPS data, the total nitrogen content of the LGF was 6.8 at%, and nitrogen itself was 0.6 at% in pyrrole, substitutive 2.4 at% and pyridine 1.3 at% states (Fig. 3a) [24,29]. In addition, the N1s spectrum in Fig. 3a was deconvoluted into four peaks, the peak which is centered at 397.7 eV is ascribable to the sp<sup>2</sup> N involved in triazine rings, whilst the contribution at 398.7 eV attributes to bridged atoms of nitrogen N-(C)<sub>3</sub> [40]. The peak at 400.2 eV may be ascribed to the =NH or –NH<sub>2</sub> groups [41]. Positive charge localization or charging effects in heterocycles can lead to the peak at 403.8 eV. As highlighted in Fig. 3b, the curve fitting of the O1s spectra generally indicates components centered at 529 and 531.6 eV, which are basically attributed to the carbon phase's surface oxygen complexes [42].

Fig. 4 shows the H<sub>2</sub>-temperature-programmed reduction (H<sub>2</sub>-TPR) profiles of the prepared catalysts: 10Co/Nb<sub>2</sub>O<sub>5</sub>, 10Co/CNT-Nb<sub>2</sub>O<sub>5</sub>, and 3Co/CNT. The catalysts were reduced at the temperature of 400 °C. In this case, the signals corresponded to the decomposition of residual cobalt nitrate at ~300–400 °C on the TPR spectra of the 10Co/Nb<sub>2</sub>O<sub>5</sub> and 10Co/CNT-Nb<sub>2</sub>O<sub>5</sub> samples. Peaks ranging from 260 to 400 °C were related to the reduction of Co<sub>3</sub>O<sub>4</sub> to CoO, and CoO was reduced to a metal at 340–410 °C [24]. The maximum absorption of hydrogen at

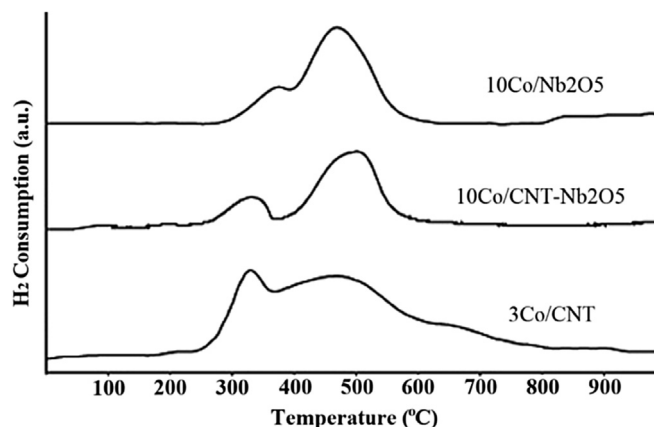


Fig. 4. H<sub>2</sub>-TPR profiles of the Co/Nb<sub>2</sub>O<sub>5</sub>, Co/CNT-Nb<sub>2</sub>O<sub>5</sub> and Co/CNT catalysts.

**Table 3**  
CO<sub>2</sub> conversion and selectivity formation of CH<sub>4</sub> and CO over Co containing catalysts.

Catalyst	Selectivity, %		CO <sub>2</sub> conversion, %
	CH <sub>4</sub>	CO	
3Co/CNT	0	0	0
3Co/CNT (activated)	22	78	13
35Co/CNT	100	0	86
10Co/CNT-Nb <sub>2</sub> O <sub>5</sub>	100	0	55
20Co/CNT-Nb <sub>2</sub> O <sub>5</sub>	100	0	71
35Co/CNT-Nb <sub>2</sub> O <sub>5</sub>	100	0	93
3Co/CNF	77	23	24
1.5Co/LGF	0	0	0
3Co/LGF	36	64	20
10Co/LGF	18	82	31
10Co/Nb <sub>2</sub> O <sub>5</sub>	100	0	35
20Co/Nb <sub>2</sub> O <sub>5</sub>	100	0	46
35Co/Nb <sub>2</sub> O <sub>5</sub>	100	0	100

Reaction conditions: T = 320 °C, P = 1 MPa, H<sub>2</sub>/CO<sub>2</sub>/He = 5:2:1 (molar ratio).

380–650 °C for 3Co/CNT is associated with the methane formation by the interaction of hydrogen with CNT [24]. For 10Co/Nb<sub>2</sub>O<sub>5</sub> sample, the maximum adsorption of hydrogen was occurred at 740–850 °C and it is connected with the reduction of stable spinel of Co/Nb<sub>2</sub>O<sub>5</sub> [43–46], and for 10Co/CNT-Nb<sub>2</sub>O<sub>5</sub> at 640–770 °C are due to both factors.

All catalysts containing more than 3 wt% of cobalt, proved to be active at > 200 °C. The main products of the reaction were methane and/or CO under the present reaction conditions. Table 3 illustrates the data on the CO<sub>2</sub> conversion and the selectivity of the catalysts at 320 °C. It is known that the activity and selectivity of catalytic hydrogenation of CO are affected by the particles size of the metal catalyst [23,47–54] and the narrow range of their distribution [48]. The highest activity of cobalt catalysts is observed at a particle size of Co equal to ~ 5–8 nm [23,54]. Wherein, the highest selectivity of methane formation from the CO hydrogenation reaction is achieved with a particle size of Co 2.5–5 nm [23].

In the present study it was found that the conversion of CO<sub>2</sub> increased with increasing metal content in the catalyst supported by all types of support (Table 3). The selectivity of methane formation was 100% in the presence of catalysts based on Nb<sub>2</sub>O<sub>5</sub> oxide and carbon-oxide CNT-Nb<sub>2</sub>O<sub>5</sub> compositions, as well as for the catalyst with a cobalt content of 35 wt%.

According to the catalytic investigations, the catalysts containing 1.5 to 3 wt% of Co obtained via impregnation and non-involuntary adsorption, it was found that 1.5Co/LGF and 3Co/CNT are not active in a wide temperature range. Studies by TEM and electronic nano-diffraction showed that cobalt was in an amorphous state and the particle size did not exceed ~4 nm (Fig. 5a). To establish the effect of the Co phase state on the CO<sub>2</sub> hydrogenation process, the 3Co/CNT catalyst was re-reduced with hydrogen at 400 °C for 4 h, and then subjected to thermal treatment at 350 °C for 2.5 h in helium current. Additionally, the data, obtained by TEM and electron diffraction methods, indicated that 3Co/CNT catalyst crystallized (Fig. 5b), and the CO<sub>2</sub> conversion was 13% at 320 °C. This fact may indicate that the reaction of reductive CO<sub>2</sub> conversion is structurally sensitive.

Unlike 3Co/CNT, the 3Co/CNF and 3Co/LGF catalysts showed activity immediately after the reduction of cobalt. According to the TEM data, the cobalt particle size was 4–5 nm (Fig. 6 a, b). When the metal content was increased to 10 wt %, the Co particle size did not change (4–5 nm), and this was not affected by the nature of the supports (CNT, CNF, or LGF) (Fig. 6 c, d). It can be assumed that at such content of metal, the particle size of Co was determined by the pore size in the carbon nanomaterials, which was previously demonstrated for Fe/carbon nanotube catalysts [55].

The CO yield was found to be significantly higher in the presence of 3Co/CNT (activated in the H<sub>2</sub> atmosphere at 400 °C for 4 h), 3Co/LGF and 10Co/LGF catalysts than the 3Co/CNF catalyst. Perhaps this is due to the functional groups existence on the surface of CNT and the presence of nitrogen-displacing atoms in the LGF's structure, which facilitated stabilization of cobalt nanoparticles and prevents their sintering during the catalytic experiments [47]. Indeed, in the example of the 10Co/CNT-Nb<sub>2</sub>O<sub>5</sub> catalyst (no stabilization centers of Co particles were created on its surface), the TEM data highlighted that the size of the cobalt particles increased from ~10 to ~23 nm after the catalytic tests (Fig. 7). It is noted that with the particle size of ~23 nm, the only CO<sub>2</sub> hydrogenation product was methane (CH<sub>4</sub>).

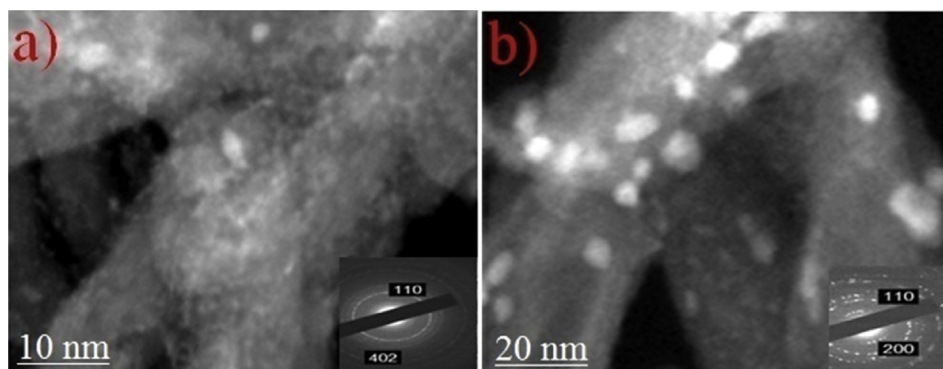


**Fig. 5.** TEM images and micro-diffraction data of the 3Co/CNT catalyst before (a) and after (b) thermal activation.

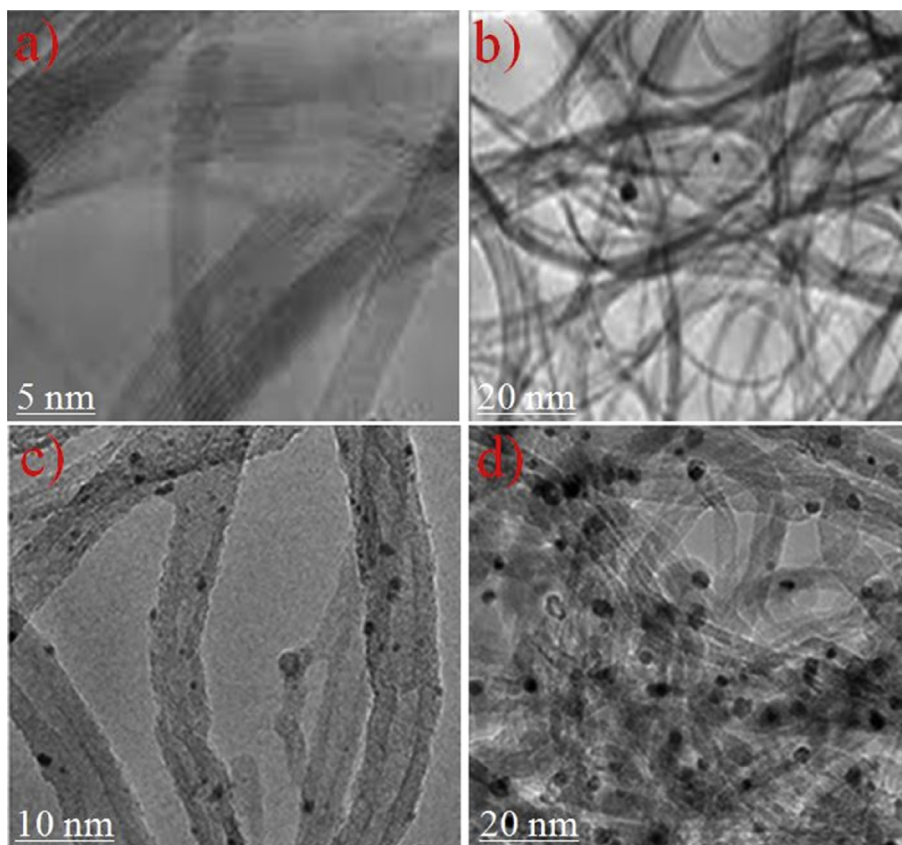


Fig. 6. TEM micrographs of the 3Co/CNF (a), 3Co/LGF (b), 10Co/CNT (c) and 10Co/LGF (d) catalysts.

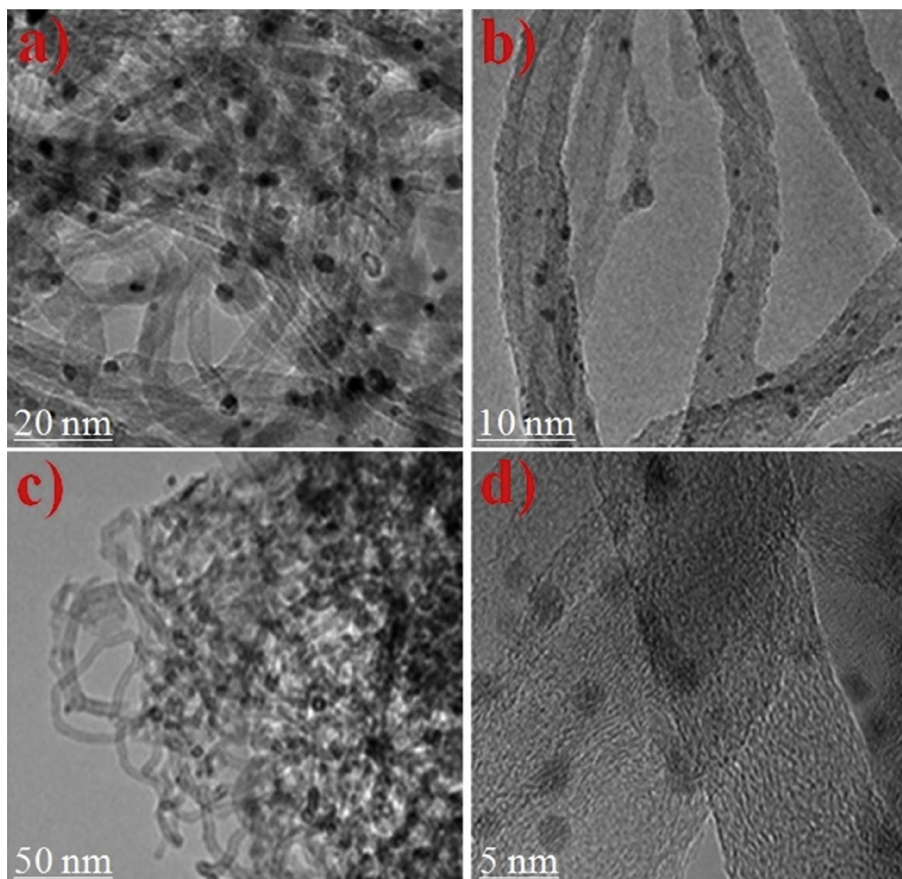


Fig. 7. TEM light and dark field images of the 10Co/CNT-Nb<sub>2</sub>O<sub>5</sub> catalyst before (a, b) and after (c, d) catalytic experiments.

Among the main factors affecting the reductive conversion of CO<sub>2</sub> in the presence of cobalt-containing catalysts with Co concentration of 1.5–35 wt%, one can single out the nature of the supports (Nb<sub>2</sub>O<sub>5</sub>, carbon nanomaterials of CNT, CNF, LGF and CNT-Nb<sub>2</sub>O<sub>5</sub>), wt content, particle size and phase state of cobalt.

The cobalt particle size (which can be assumed to be determined by the pore size in the carbon material) was ~4 nm for the catalysts Co/CNT, Co/CNF, Co/MHF with 1.5–10 wt% of Co content and the products were methane and CO. With increasing Co concentration up to 20 wt% and higher, the only CO<sub>2</sub> hydrogenation product was methane in the presence of catalysts based on oxide Nb<sub>2</sub>O<sub>5</sub> and carbon-oxide compositions CNT-Nb<sub>2</sub>O<sub>5</sub>.

The Co/CNT and Co/LGF catalysts, with 1.5–3 wt% content of Co, are not active. According to TEM and nanodiffraction analyses, it was indicated that the cobalt particles in these samples are amorphous. It has been proved that such catalysts can be activated by crystallization during thermal treatment.

The surface modification of carbon materials by oxygen groups or by introduction of graphene sheets of the nitrogen atoms into the surface structure increases the stability of cobalt-containing catalysts. In this regard, to reduce the deactivation degree of Co nanoparticles on the surface of the supports, it is proposed to use carboxylated CNTs and LGF hetero-substituted by nitrogen atoms.

#### 4. Conclusion

The Co supported on CNT, CNF, LGF, CNT-Nb<sub>2</sub>O<sub>5</sub> and Nb<sub>2</sub>O<sub>5</sub> catalysts have been prepared by the impregnation method of the supports with a solution of cobalt nitrate and tested for CO<sub>2</sub> hydrogenation to value-added products. The main CO<sub>2</sub> hydrogenation products were CH<sub>4</sub> and CO. 3Co/CNT (activated in the H<sub>2</sub> atmosphere at 400 °C for 4 h), 3Co/LGF and 10Co/LGF catalysts have led to higher CO yield than 3Co/CNF catalyst. Increase of Co concentration in the catalysts based on Nb<sub>2</sub>O<sub>5</sub> and CNT-Nb<sub>2</sub>O<sub>5</sub> led to formation of CH<sub>4</sub> only. The Co/CNT (3 wt% of Co content) and Co/LGF (1.5 wt% of Co content) catalysts were not active for hydrogenation of CO<sub>2</sub> to liquid/or chemical products due to the cobalt particles in these samples were amorphous, but according to obtained experimental data, these catalysts can be activated by application of thermally induced crystallization of cobalt.

Introduction of nitrogen atoms into graphene sheets or surface functionalizations of the carbon nanomaterials with oxygen containing groups amplify the stability and effectiveness of the Co containing catalysts. Hence, it is recommended that nitrogen-heterosubstituted low-layered graphite fragments and carboxylated carbon nanotubes should be applied to reduce the deactivation degree of the cobalt nanoparticles on the surface of the support.

#### Acknowledgment

The work was carried out with financial support from the Ministry of Education and Science of the Russian Federation in the framework of Increase Competitiveness Program of NUST «MISIS» (No K4-2016-054), implemented by a governmental decree dated 16th of March 2013, N 211.

#### References

- [1] C. Le Quere, et al., Global carbon budget 2016, *Earth Syst. Sci. Data* 8 (2016) 1–45.
- [2] B. Hu, C. Guild, S.L. Suib, Thermal, electrochemical, and photochemical conversion of CO<sub>2</sub> to fuels and value-added products, *J. CO<sub>2</sub> Util.* 1 (2013) 18–27.
- [3] M. Cokoja, C. Bruckmeier, B. Rieger, W.A. Herrmann, F.E. Kühn, Transformation of carbon dioxide with homogeneous transition-metal catalysts: a molecular solution to a global challenge? *J. Chem. Int. Ed.* 50 (2011) 8510–8537.
- [4] H.M. Galvis, J.H. Bitter, C.B. Khare, M. Ruitenbeek, A.I. Dugulan, K.P. de Jong, Supported iron nanoparticles as catalysts for sustainable production of lower Olefins, *J. Sci.* 335 (2012) 835–838.
- [5] G. Centi, E.A. Quadrelli, S. Perathoner, Catalysis for CO<sub>2</sub> conversion: a key technology for rapid introduction of renewable in the value chain of chemical industries, *J. Energy Environ. Sci.* 6 (2013) 1711–1731.
- [6] H. Li, P.H. Opgenorth, D.G. Wernick, S. Rogers, T.Y. Wu, W. Higashide, P. Malati, Y.X. Huo, K.M. Cho, J.C. Liao, Integrated electromicrobial conversion of CO<sub>2</sub> to higher alcohols, *J. Sci.* 335 (2012) 1596.
- [7] L. Yuan, Y.J. Xu, Photocatalytic conversion of CO<sub>2</sub> into value added and renewable fuels, *J. Appl. Surf. Sci.* 342 (2015) 154–167.
- [8] H. Lei, Z. Hou, J. Xie, Hydrogenation of CO<sub>2</sub> to CH<sub>3</sub>OH over CuO/ZnO/Al<sub>2</sub>O<sub>3</sub> catalysts prepared via a solvent-free routine, *J. Fuel* 164 (2016) 191–198.
- [9] C.G. Visconti, M. Martinelli, L. Falbo, L. Fratolocchi, CO<sub>2</sub> hydrogenation to hydrocarbons over CO and Fe-based Fischer-Tropsch catalysts, *J. Catal. Today* 277 (2016) 161–170.
- [10] Q. Zhang, W. Deng, Y. Wang, Recent advances in understanding the key catalyst factors for Fischer-Tropsch synthesis, *J. Energy Chem.* 22 (2013) 27–38.
- [11] E. Balaraman, C. Gunanathan, J. Zhang, L. Shimon, D. Milstein, Efficient hydrogenation of organic carbonates, carbamates, and formates indicates alternative routes to methanol based on CO<sub>2</sub> and CO, *J. Nat. Chem.* 3 (2011) 609–614.
- [12] C.M. Rayner, The potential of carbon dioxide in synthetic organic chemistry, *J. Org. Process Res. Dev.* 11 (2007) 121–132.
- [13] S.H. Kim, K.H. Kim, S.H. Hong, Carbon dioxide capture and use: organic synthesis using carbon dioxide from exhaust gas, *J. Angew. Chem.* 126 (2014) 790–793.
- [14] G. Yuan, C. Qi, Q. Wu, H. Jiang, Recent advances in organic synthesis with CO<sub>2</sub> as C<sub>1</sub> synthon, *J. Curr. Opin. Green Sustain. Chem.* 3 (2017) 22–27.
- [15] G. Centi, S. Perathoner, Heterogeneous catalytic reactions with CO<sub>2</sub>: status and perspectives, *J. Stud. Surf. Sci. Catal.* 153 (2004) 1–8.
- [16] M. Behrens, Heterogeneous catalysis of CO<sub>2</sub> conversion to methanol on copper surfaces, *J. Angew. Chem. Int. Ed.* 53 (2014) 12022–12024.
- [17] S. Saeidi, N. Amin, M.R. Rahimpour, Hydrogenation of CO<sub>2</sub> to value-added products—a review and potential future developments, *J. CO<sub>2</sub> Util.* 5 (2014) 66–81.
- [18] K. Yu, I. Curcic, J. Gabriel, S. Tsang, Recent advances in CO<sub>2</sub> capture and utilization, *J. Chem. Sus. Chem.* 1 (2008) 893–899.
- [19] H. Muller, K. Deller, B. Despeyroux, E. Peldszus, Catalytic purification of waste gases containing chlorinated hydrocarbons with precious metal catalysts, *J. Catal. Today* 17 (1993) 383–390.
- [20] M. Martinelli, C. Visconti, L. Lietti, P. Forzatti, C. Bassano, P. Deiana, CO<sub>2</sub> reactivity on Fe-Zn-Cu-K Fischer-Tropsch synthesis catalysts with different K-loadings, *J. Catal. Today* 228 (2014) 77–88.
- [21] R.B. Anderson, *The Fischer-Tropsch Synthesis*, Academic Press Inc., New York, 1984.
- [22] A.P. Stynberg, M.E. Dry, *Fischer-Tropsch Technology*, Elsevier Ltd, Amsterdam, 2004.
- [23] G.L. Bezemer, J.H. Bitter, H. Kuipers, H. Oosterbeek, J.E. Holewijn, X. Xu, F. Kapteijn, A. van Dillen, K.P. de Jong, Cobalt particle size effects in the Fischer-Tropsch reaction studied with carbon nanofiber supported catalysts, *J. Am. Chem. Soc.* 128 (2006) 3956–3964.
- [24] M. Trepanier, A. Tavasoli, A.K. Dalai, N. Abatzoglou, Fischer-Tropsch synthesis over carbon nanotubes supported cobalt catalysts in a fixed bed reactor: influence of acid treatment, *J. Fuel Process. Technol.* 90 (2009) 367–374.
- [25] E.P. Barrett, L.G. Joyner, P.P. Halenda, The determination of pore volumes and area distributions in porous substances. I. Computations from nitrogen isotherms, *J. Am. Chem. Soc.* 73 (1951) 373–380.
- [26] X. Qi, Ch Qin, W. Zhong, Ch Au, X. Ye, Y. Du, Large-scale synthesis of carbon nanomaterials by catalytic chemical vapor deposition: a review of the effects of synthesis parameters and magnetic properties, *J. Mater.* 3 (2010) 4142–4174.

- [27] R.K. Rana, X.N. Xu, Y. Yeshurun, A. Gedanken, Preparation, texture, and magnetic properties of carbon nanotubes/nanoparticles doped with cobalt, *J. Phys. Chem. B* 106 (2002) 4079–4084.
- [28] H. Wang, T. Maiyalagan, X. Wang, Review on recent progress in nitrogen-doped graphene: synthesis, characterization, and its potential applications, *J. ACS Catal.* 2 (2012) 781–794.
- [29] L. Kumari, T. Zhang, G.H. Du, W.Z. Li, Q.W. Wang, A. Datye, K.H. Wu, Thermal properties of CNT-Alumina nanocomposites, *J. Compos. Sci. Technol.* 68 (2008) 2178–2183.
- [30] S.R.J. Saudres, M. Monteiro, F. Rizzo, The oxidation behavior of metals and alloys at high temperatures in atmospheres containing water vapour: a review, *J. Prog. Mater. Sci.* 53 (2008) 775–837.
- [31] J.F. Hong, K. Mato, S. Ronald, H. Dietrich, N. Kornelius, Z. Margit, G. Ulrich, Influence of surface diffusion on the formation of hollow nanostructures induced by the kirkendall effect: the basic concept, *J. Nano Lett.* 7 (2007) 993–997.
- [32] C.M. Wang, D.R. Baer, L.E. Thomas, J.E. Amonette, Void formation during early stages of passivation: initial oxidation of iron nanoparticles at room temperature, *J. Appl. Phys.* 98 (2005) 1–7.
- [33] F. Joucken, Y. Tison, J. Lagoute, J. Dumont, D. Cabosart, B. Zheng, V. Repain, C. Chacon, Y. Girard, A.R. Botello-Mendez, S. Rousset, R. Sporken, J.C. Charlier, L. Henrard, Localized state and charge transfer in nitrogen-dropped graphene, *J. Phys. Rev. B* 85 (2012), 161408(1) – 161408(4).
- [34] B. Guo, Q. Liu, E. Chen, H. Zhu, L. Fang, J. Gong, Controllable N-doping of graphene, *J. Nano Lett.* 10 (2010) 4975–4980.
- [35] H. Gao, L. Song, W. Guo, L. Huang, D. Yang, F. Wang, Y. Zuo, X. Fan, Z. Liu, W. Gao, R. Vajtai, K. Hackenberg, P.M. Ajayan, A simple method to synthesize continuous large area nitrogen-doped graphene, *J. Carbon* 50 (2012) 4476–4482.
- [36] E.A. Skryleva, Y.N. Parkhomenko, I.M. Karnaukh, E.A. Zhukova, A.R. Karaeva, V.Z. Mordkovich, XPS characterization of MWCNT and C<sub>60</sub>-based composites, *J. Fuller. Nano. Carbon Nanostruct.* 24 (2016) 535–540.
- [37] A. Rasheed, J. Howe, M. Dadmun, P. Britt, The efficiency of the oxidation of carbon nanofibers with various oxidizing agents, *J. Carbon* 45 (2007) 1072–1080.
- [38] A.A. Novakova, A.N. Antonov, T.S. Gendler, E.A. Kolesnikov, I.I. Puzik, V.V. Levina, The influence of surface active substances various concentrations on goethite nanoparticles magnetic properties, *J. Solid State Phenomena* 190 (2012) 447–450.
- [39] A.Z. Arifin, Y.M. Ambar, A.F.H. Abdul, S.M.Y. Meor, A.B. Ismail, K. Nizar, J.A. Rashid, S.M. Azwadi, R.M. Fariz, Nanomaterials – Synthesis and Characterization, *Trans Tech Publications Ltd*, 2012.
- [40] Q. Xiang, J. Yu, M. Jaroniec, Preparation and enhanced visible-light photocatalytic H<sub>2</sub>-production activity of graphine/C<sub>3</sub>N<sub>4</sub> composites, *J. Physic. Chem. C* 115 (2011) 7355–7363.
- [41] B. Zhao, Z. Han, K. Ding, The N-H functional group in organometallic catalysis, *J. Angew. Chem.* 52 (2013) 4744–4788.
- [42] O. Akhavan, Graphene nanomesh by ZnO nanorod photocatalysis, *J. ACS Nano* 4 (2010) 4174–4180.
- [43] V. Parvulescu, M. Ruwetb, P. Grangeb, V.I. Parvulescu, Preparation, characterization and catalytic behavior of cobalt-niobia catalysts, *J. Mol. Catal. A Chem.* 135 (1998) 75–88.
- [44] F.B. Noronha, A. Frydman, D.A.G. Aranda, C. Perez, R.R. Soares, B. Morawek, D. Castner, C.T. Campbell, R. Frety, M. Schmal, The promoting effect of noble metal addition on niobia-supported cobalt catalysts, *J. Catal. Today* 28 (1996) 147–157.
- [45] F. Mendes, C. Perez, F. Noronha, C. Souza, D. Cesar, H. Freund, M. Schimal, Fischer-tropsch synthesis on anchored Co/Nb<sub>2</sub>O<sub>5</sub>/Al<sub>2</sub>O<sub>3</sub> catalysts: the nature of the surface and the effect on chain growth, *J. Phys. Chem. B* 110 (2006) 9155–9163.
- [46] M. Schimal, H. Freund, Towards an atomic level understanding of niobia based catalysts and catalysis by combining the science of catalysis with surface science, *J. An. Acad. Bras. Cienc* 81 (2009) 297–318.
- [47] B. Fernandez, S. Goyanes, G.H. Rubiolo, I. Mondragon, M.A. Corcuera, A. Eceiza, Surface modification of multiwalled carbon nanotubes via esterification using a biodegradable polyol, *J. Nanosci. Nanotechnol.* 9 (2009) 6064–6071.
- [48] A. Karimi, B. Nasernejad, M. Rashidi, A. Tavasoli, M. Pourkhalil, Functional group effect on carbon nanotube (CNT)-supported cobalt catalysts in Fischer-Tropsch synthesis activity, selectivity and stability, *J. Fuel* 117 (2014) 1045–1051.
- [49] J.P. den Breejen, P.B. Radstake, G.L. Bezemer, J.H. Bitter, V. Froseth, A. Holmen, F. Kapteijn, K.P. de Jong, On the origin of the cobalt particle size effects in Fischer-Tropsch catalysis, *J. Am. Chem. Soc.* 131 (2009) 7197–7203.
- [50] G.L. Bezemer, T.J. Remans, A.P. van Bavel, A. Dugulan, Direct evidence of water-assisted sintering of cobalt on carbon nanofiber catalysts during simulated Fischer-Tropsch conditions revealed with in situ Mossbauer Spectroscopy, *J. Am. Chem. Soc.* 132 (2010) 8540–8541.
- [51] G. Melaet, W.T. Ralston, Ch Li, S. Alayoglu, K. An, N. Musselwhite, B. Kalkan, G.A. Somorjai, Evidence of highly active cobalt oxide catalyst for the Fischer-tropsch synthesis and CO<sub>2</sub> hydrogenation, *J. Am. Chem. Soc.* 136 (2014) 2260–2263.
- [52] P. Munnik, P.E. de Jongh, K.P. de Jong, Control and impact of the nanoscale distribution of supported cobalt particles used in Fischer-Tropsch catalysis, *J. Am. Chem. Soc.* 136 (2014) 7333–7340.
- [53] N.E. Tsakoumis, J.C. Walmsley, M. Ronning, W. van Beek, E. Rytter, A. Holmen, Evaluation of reoxidation thresholds for  $\gamma$ -Al<sub>2</sub>O<sub>3</sub>-supported cobalt catalysts under Fischer-Tropsch synthesis conditions, *J. Am. Chem. Soc.* 139 (2017) 3706–3715.
- [54] A. Pour, E. Hosaini, A. Tavasoli, A. Behroozsarand, F. Dolati, Intrinsic kinetics of Fischer-Tropsch synthesis over Co/CNT catalyst: effects of metallic cobalt particle size, *J. Nat. Gas Sci. Eng.* 21 (2014) 772–778.
- [55] R.M. Abbaslou, J. Soltan, A.K. Dalai, Effect of nanotubes pore size on the catalytic performances of iron catalysts supported on carbon nanotubes for Fischer-Tropsch synthesis, *J. Appl. Catal. A General* 379 (2010) 129–134.